

Optimizing Topological Switching in Confined 2D-Xene Nanoribbons via Finite-Size Effects

Muhammad Nadeem,^{†,‡} Chao Zhang,[¶] Dimitrie Culcer,^{§,||} Alex R. Hamilton,^{§,||}
Michael S. Fuhrer,^{⊥,#} and Xiaolin Wang^{†,‡}

[†]*Institute for Superconducting and Electronic Materials (ISEM), Australian Institute for Innovative Materials (AIIM), University of Wollongong, Wollongong, New South Wales 2525, Australia.*

[‡]*ARC Centre of Excellence in Future Low-Energy Electronics Technologies (FLEET), University of Wollongong, Wollongong, New South Wales 2525, Australia*

[¶]*School of Physics, University of Wollongong, Wollongong, NSW 2522, Australia*

[§]*School of Physics, University of New South Wales, Sydney 2052, Australia.*

^{||}*ARC Centre of Excellence in Future Low-Energy Electronics Technologies (FLEET), University of New South Wales, Sydney 2052, Australia.*

[⊥]*School of Physics and Astronomy, Monash University, Clayton, Victoria 3800, Australia.*

[#]*ARC Centre of Excellence in Future Low-Energy Electronics Technologies (FLEET), Monash University, Clayton, Victoria 3800, Australia.*

E-mail:

Abstract

In a blueprint for topological quantum electronics, edge state transport in a topological insulator material can be controlled by employing a gate-induced topological quantum phase transition. While finite-size effects have been widely studied in 2D-Xenes, less attention has been devoted to finite-size effects on the gate-induced topological switching in spin-orbit coupled 2D-Xene nanoribbons. Here, by studying width dependence of electronic properties via a tight binding model, we demonstrate that finite-size effects can be used to optimize both the spin-orbit interaction induced barrier in the bulk and the gate-controlled quantized conductance on the edges of zigzag-Xene nanoribbons. The critical electric field required for switching between gapless and gapped edge states reduces as the width decreases, without any fundamental lower bound. This size dependence of the threshold voltage stems from a unique feature of zigzag-Xene nanoribbons: width and momentum dependent tunability of the gate-induced coupling between overlapping spin-filtered chiral states on the two edges. Furthermore, when the width of zigzag-Xene nanoribbons is smaller than a critical limit, topological switching between edge states can be attained without bulk band gap closing and reopening. This is primarily due to the quantum confinement effect on the bulk band spectrum which increases nontrivial bulk band gap with decrease in width. Such reduction in threshold voltage accompanied by enhancement in bulk band gap overturns the conventional wisdom of utilizing wide channel and narrow gap semiconductors for reducing threshold voltage in standard field effect transistor analysis and paves the way towards next-generation low-voltage topological quantum devices.

Keywords: 2D Topological Insulators, Topological switching, Low-voltage field effect transistor, Finite-size effects, Quantum confinement, Zigzag-Xenes nanoribbons.

Two-dimensional topological insulators are promising materials for topological quantum electronics devices where edge state transport can be controlled by a gate-induced electric field.¹ In general, edge state transport can be controlled either by a perpendicular electric field, which drives a topological phase transition via bulk band gap closing and reopening^{2–10} or via inter-edge tunnelling between gapped edge states, assisted by a transverse electric field.¹¹ In the latter case, though a very weak transverse electric field is sufficient to induce inter-edge tunneling, edge state conductance quantization may remain a challenge constraining the geometry of topological insulator ribbons.¹¹ On the other hand, in the former case, the strength of the gate electric field required for topological switching depends upon the strength of quantum mechanical perturbations, such as the spin-orbit interaction and BHZ mass term,^{12,13} which reflect the bulk band topology and therefore lead to a quantized edge state conductance. In this class, numerous theoretical proposals for 2D topological insulator materials have been put forward, which exhibit electrically-driven topological quantum phase transitions, such as staggered sublattice potentials,^{2,8,10} mirror symmetry breaking,³ and the Stark effect.^{4–7,9}

For both the study of fundamental phenomena in the laboratory and the device applications, it is crucial to investigate the fundamental topological features and edge state transport in finite-size geometries in various topological insulators. Apart from the relativistic quantum mechanical phenomenon of spin-orbit interaction (SOI) which plays a central role in characterizing the bulk band topology, finite-size geometry incorporates two additional critical phenomena: quantum confinement effects and inter-edge coupling between spin-filtered chiral edge states. Finite-size effects have been studied for various topological insulator systems via the thickness dependence of surface electronic dispersion in thin films of 3D topological insulators^{14–16} and Dirac semimetals^{5,9} and the width dependence of edge state electronic dispersion in 2D topological insulator materials such as HgTe,¹⁷ TMDC-1T',¹⁸ and 2D-Xenes.^{19–24}

Among 2D topological insulator materials, quantum spin Hall (QSH) insulators with

honeycomb lattice structures terminated on zigzag edges are a special class where spin-filtered chiral modes are intertwined with the intrinsic band topology of pristine honeycomb lattice structure. After seminal work by Kane-Mele^{25,26} on graphene, it has been shown that other 2D-Xene nanoribbons (Si,Ge,Sn, and P,As,Sb,Bi) with honeycomb lattices are also QSH insulators.²⁷⁻³³ In zigzag Xene nanoribbons (ZXNRs), the intrinsic band topology, characterized by a non-vanishing winding number, leads to energy-zero flat bands in the nontrivial regime of the first Brillouin zone. The sublattice resolved intrinsic SOI, modelled through next-nearest hopping,^{25,26} disperses these localized modes into spin-filtered chiral edge states. Unlike these various 2D topological insulator materials, in which edge state crossing and anti-crossing points coexist, and in which hybridization due to inter-edge overlapping opens an energy gap and leads to a gapped edge state spectrum, spin-filtered chiral edge states in ZXNRs remain gapless and protected against backward scattering even with finite inter-edge overlapping in ultra-narrow ribbons, i.e., a 2D QSH material turns into 1D topological metal. Such robustness is the consequence of different momentum space locations for edge state crossings (at TRIM $k = \pi$) and anti-crossings (around valleys $k = K/K'$).

While finite-size effects have been widely studied in 2D-Xenes,¹⁹⁻²⁴ effects of quantum confinement and momentum-dependent inter-edge overlapping on the gate-induced topological switching in spin-orbit coupled ZXNRs hosting QSH phase have received comparatively less attention. Here we demonstrate that both the spin-orbit interaction induced barrier in the bulk and the gate-controlled quantized conductance on the edges can be optimized via finite-size effects. By studying width dependence of electronic properties in ZXNRs via tight binding model, it is inferred that the momentum space location of the anti-crossing points, the magnitude of the overlap integral between spin-filtered edge states on the two sides, and the threshold gate voltage are intertwined and are directly associated with the width of ZXNRs. These fundamental features enable optimal control of edge state transport via spin-filtered chiral modes.

We demonstrate explicitly that such an optimization is indebted to a series of non-trivial

quantum mechanical phenomena associated with the geometric structure of ZXNRs. Firstly, the edge state wave functions at the crossing point are independent of the edge termination and hence remain insensitive to electric fields. On the other hand, edge state wave functions and the gate-induced coupling between overlapping edge states across anti-crossing points are strongly dependent on the particular edge termination and hence can be tuned via a gate electric field. Secondly, with a decrease in width, the momentum space location of the edge state anti-crossing points move away from the valleys $k = K/K'$ towards the TRIM $k = \pi$. Furthermore, at particular momenta around the anti-crossing points, the magnitude of the inter-edge overlap increases with decreasing width. As a result, gate-induced coupling between spin-filtered chiral edge states is enhanced as the ZXNR width is reduced. It shows that finite-size effects on the edge spectrum play a central role in optimizing the gate-controlled edge state transport, such that width-dependent and momentum-dependent tunability of the inter-edge coupling reduces the critical gate electric field.

On the other hand, quantum confinement enhances the topological bulk band gap and hence the energy spacing between the bulk subbands and the edge states, which in turn leads to topological switching between gapless and gapped edge states without bulk band gap closing. It is important to note that the threshold reduction could in principle be achieved with a built-in electric field due to static charges. However, for a fixed SOI in ZXNRs, a simple enhancement of the built-in electric field also reduces the topological band gap in the QSH phase, which may be detrimental to quantized edge state conductance. In this regard, size-dependent and momentum-dependent tunability of gate-induced inter-edge coupling is a novel mechanism that reduces the critical gate electric field even as the topological bulk band gap is enhanced by quantum confinement. Both of these finite-size phenomena, central to the control of edge state transport, are completely missing in wide ZXNRs: there gate-induced coupling is only possible at the valleys, and the topological phase transition is accompanied by bulk band gap closing and reopening.

These features make quantum confined spin-orbit coupled ZXNRs special for topological

quantum devices, enabling optimal gate-controlled transport through edge state channels via finite-size effects on the electronic properties. Reduction in threshold gate voltage accompanied by enhancement in bulk band gap overturns the conventional wisdom of utilizing wide channel and narrow gap semiconductors for reducing threshold gate voltage in standard field effect transistor analysis, other than negative capacitance mechanism.³⁴ Furthermore, the advantage of utilizing ultra-narrow ZXNRs is two-fold: (i) availability of large edge state conducting modes for enhanced signal-to-noise ratio via multiple edge state channels, and (ii) optimized geometry for topological electronic devices, as shown in figure 1 (b).

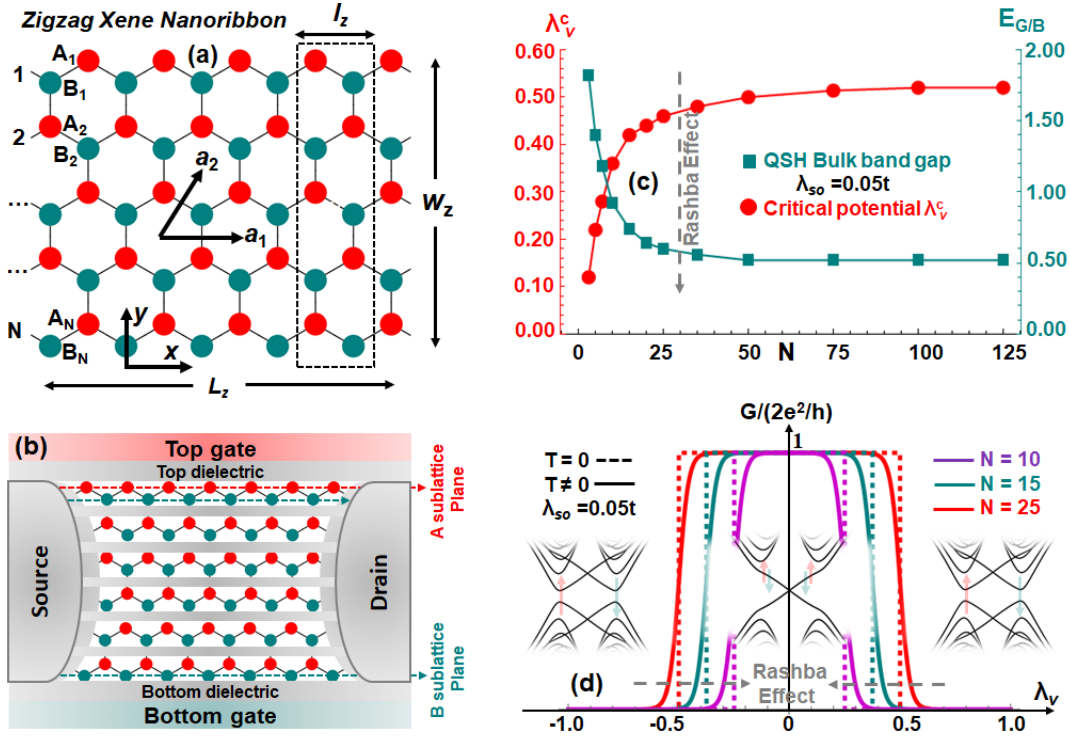


Figure 1: **Optimization of electronic properties in quantum confined ZXNRs.** (a) A ZXNR with lattice parameters. (b) Transistor geometry configuring quantum confined ZXNRs. An array of ZXNRs, set apart by trivial insulating layers/wires along vertical/lateral direction, is sandwiched between top and bottom gates separated by top and bottom dielectrics. (c) Topological switching via electric field effect is assisted by the finite-size effect which lowers the critical gate electric field as the width of ZXNRs decreases even though nontrivial bulk band gap increases with decrease in the width of ZXNRs. (d) Quantized edge state conductance and the critical gate electric field for $N = 10, 15,$ and 25 . Here, Rashba SOI is ignored for simplicity. When topological quantum field effect is also incorporated, Rashba SOI induces a downward shift in both the bulk band gap and the threshold gate voltage.

Finite-size effect assisted topological switching

Figure 1 (a) shows a ZXNR, composed of N zigzag lines where the primitive lattice vectors are represented by $a_1 = a_0(1, 0)$ and $a_2 = a_0(1/2, \sqrt{3}/2)$, d_z represents the buckling length, while the vertical dashed rectangle (composing dimer line of A and B sublattice sites) represents the unit cell for ZXNR. The length of unit cell (dimer line) represents the width $W_z = \sqrt{3}N_d a_0/4$ of ZXNR where $N_d = 2N$ represents the number of sites in the dimer line. The length of ZXNR, $L_z = D l_z$ where D represents the number of dimer lines and l_z is the width of dimer line, can be written as a function of N_z , number of sites in the zigzag line, as $L_z = N_z a_0/2$.

With energy-zero modes in pristine case and the spin-filtered chiral edge states in the spin-orbit coupled case, ZXNRs are promising materials with a display of unique physical characteristics associated with the intrinsic band topology and the finite-size effects on gate-induced topological switching. To simulate this, the dependence of electronic properties on the width of ZXNRs can be characterized by the following tight-binding model Hamiltonian^{25,26}

$$\begin{aligned}
 H = & t \sum_{\langle ij \rangle \alpha} c_{i\alpha}^\dagger c_{j\alpha} + i\lambda_{so} \sum_{\langle\langle ij \rangle\rangle \alpha\beta} v_{ij} c_{i\alpha}^\dagger s_{\alpha\beta}^z c_{j\beta} \\
 & + \frac{\lambda_v}{2} \sum_{i\alpha} c_{i\alpha}^\dagger v_i c_{i\alpha} + i\lambda_R(E_z) \sum_{\langle ij \rangle \alpha\beta} c_{i\alpha}^\dagger (\mathbf{s}_{\alpha\beta} \times \hat{\mathbf{d}}_{ij})_z c_{j\beta},
 \end{aligned} \tag{1}$$

where first term is the nearest neighbour hopping generating Dirac dispersion in the vicinity of valleys K(K') while the second term is the intrinsic Kane-Mele type SOI ($\lambda_{so} = \Delta_{so}/3\sqrt{3}$) which opens nontrivial QSH bulk band gap^{25,26} and induces topologically protected spin-filtered chiral edge states. The third term represents the staggered sublattice potential induced by gate electric field ($E_v = \lambda_v/\alpha_v$ where α_v is the buckling dependent parameter) which drives QSH phase into trivial insulating phase - termed here as topological switching. The fourth term is the spin-mixing Rashba SOI associated with the gate electric field.^{25,26,35}

Here $c_{i\alpha}^\dagger$ ($c_{i\alpha}$) is the creation (annihilation) electron operator with spin polarization $\alpha = \uparrow$

, \downarrow on site i , the Pauli matrix s^z describes the electron intrinsic spin while $s_{\alpha\beta}^z$ are the corresponding matrix elements describing the spin polarization α and β on sites i and j , $v_i = +1(-1)$ for sublattice A (B), and $v_{ij} = \mathbf{d}_{ik} \times \mathbf{d}_{kj} = \pm 1$ connects sites i and j on sublattice A (B) via the unique intermediate site k on sublattice B (A). The nearest-neighbour bond vectors \mathbf{d}_{ik} and \mathbf{d}_{kj} connect the i (k) and k (j) sites on the A and B sublattices.

To begin with, by numerically diagonalizing the tight binding model, we study the finite-size effects on the pristine and spin-orbit coupled ZXNRs by varying the width of ZXNRs. In pristine case, as shown in figure 2 (a), intrinsic topology of honeycomb lattice structure leads to strongly localized energy-zero flat edge states between valleys K and K', $\Delta k_x = K - K' = 2\pi/3a_0$, a nontrivial regime of first Brillouin zone characterized by non-vanishing winding number. Intrinsic SOI drives pristine ZXNRs into the QSH phase and disperses these energy-zero flat edge states into spin-filtered chiral edge modes, as shown in figure 2 (b). Due to the presence of both time-reversal and inversion symmetry, edge states are Kramers pairs, forming a four-fold degenerate Dirac point at the edge state crossing point, TRIM, $k_x = \pi$. Figure 2 (c) shows that when a gate electric field is applied, Kramers partners split along the energy axis while the two-fold degenerate Dirac points in the spin down and spin up sectors move towards the corners of the nontrivial regime, valleys K and K' respectively. As a result, due to spin-valley locking, ZXNRs show spin-polarized semi-metallic behaviour at a critical point where $\lambda_v = \lambda_v^c$. When the strength of the staggered sublattice potential exceeds a threshold limit, the Dirac points in both spin sectors are gapped out at the anti-crossing points and the system enters into trivial regime.

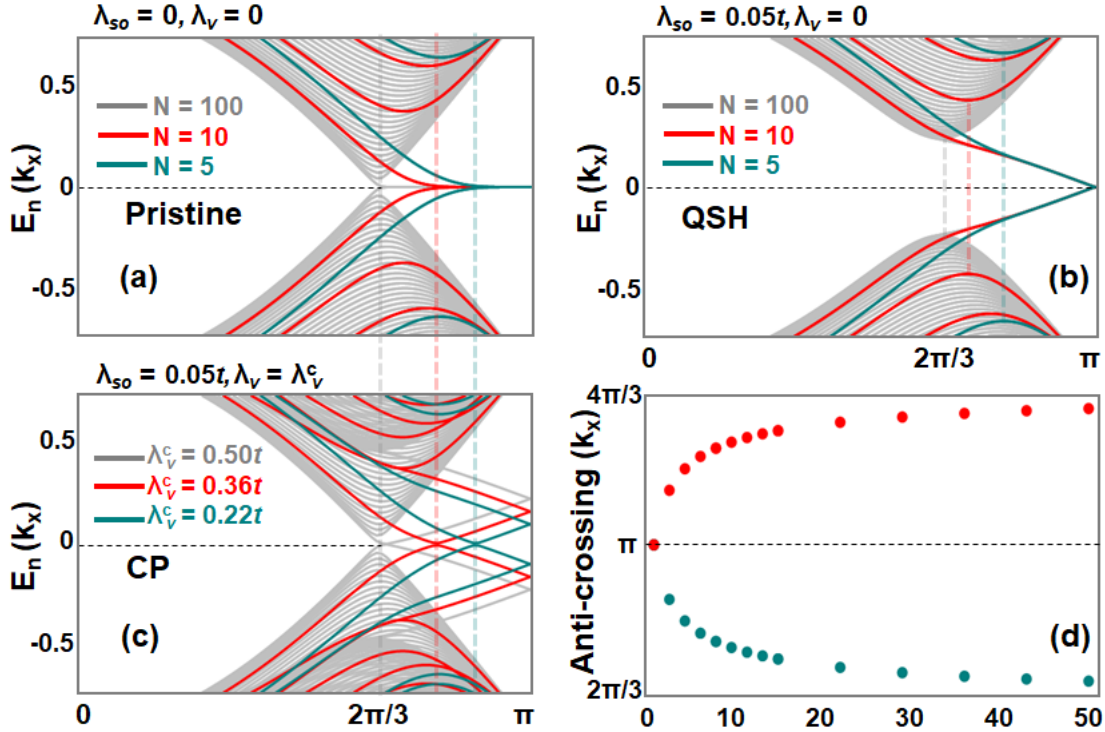


Figure 2: **Finite-size effect assisted topological switching in quantum confined ZXNRs.** (a-c) Width dependence of one-dimensional electronic band dispersion for pristine ZXNRs hosting localized energy-zero edge states (a), spin-orbit coupled ZXNRs hosting QSH phase (b), and the gate induced critical point in spin-orbit coupled ZXNRs(c). In wide ZXNRs ($N = 100$) anti-crossing point lies at the valley ($k_x = 2\pi/3$) and the critical gate electric field reads $E_c = 2\Delta_{so}/\alpha_v$. In narrow quantum confined ZXNRs ($N = 10, 5$), anti-crossing point moves from valley towards TRIM $k_x = \pi$ and the critical gate electric field reduces from the SOI driven barrier, $E_c < 2\Delta_{so}/\alpha_v$. Moreover, around anti-crossing points, the energy spacing between edge states and the bulk subbands increases with decrease in width of ZXNRs. Such an increase in the bulk band gap shows that topological switching is not accompanied by bulk band gap closing and reopening in quantum confined ZXNRs. (d) Width dependence of momentum space location of anti-crossing point. Here we set $a_0 = t = 1$ and $\lambda_R = 0$.

The bulk and edge state electronic band dispersion, obtained via numerical diagonalization of the tight binding model, show a number of counter-intuitive features depending upon the width of ZXNRs, which may prove to be interesting for both fundamental and the novel device applications in topological electronics.

From 2D QSH insulator to 1D topological metal

The trademark of spin-orbit coupled ZXNRs, namely spin-filtered QSH chiral edge states in 2D sheets, remains protected even when the system becomes effectively 1D and the QSH effect is no longer well defined. That is, as shown in figure 2(b), (i) the spin-filtered chiral edge states remain gapless even for ultra-narrow ribbons and (ii) the bulk band gap increases with decrease in width. It implies that as one makes the ZXNR narrower, it retains its topological character, i.e. has well defined 1D metallic modes associated with the edges, each with spin-momentum locking, and the bulk band gap grows. This non-intuitive result in ZXNRs seems interesting and differentiates ZXNRs from all other 2D topological insulators. In general, the effect of quantum confinement in other 2D topological insulators is to push the system towards a large-gap conventional insulator. However, in the spin-orbit coupled ZXNRs, the topological edge states remain stable as one goes to narrow ribbons - one retains the large bulk band gap and hence a large energy separation between the edge states and the bulk bands. So a narrow ZXNR remains a robust 1D topological metal characterized by a non-vanishing winding number associated with the intrinsic band topology.

This observation can be understood from fundamental quantum mechanical considerations in narrow ZXNRs: sublattice-resolved intrinsic SOI, quantum confinement, and the longitudinal momentum-dependent inter-edge coupling. First of all, both the nontrivial bulk band gap and the dispersing spin-filtered chiral edge states are indebted to the sublattice-resolved intrinsic SOI, i.e., next-nearest hopping localizes the bulk electrons while the electrons traversing along the edges remain effectively free. This SOI induced mechanism remains true, irrespective of the ZXNR width. In addition, even in the 1D limit, as discussed below, the protection of spin-filtered chiral edge modes is guaranteed by the vanishing inter-edge coupling at TRIM $k_x = \pi$. On the other hand, the enhancement of topological bulk band gap is because of quantum confinement effect on the bulk band spectrum. As shown in figure 1(c), in the absence of gate potential, while bulk band varies as $E_{G/B} = |2\Delta_{so}|$ in the wide ZXNRs, bulk band gap varies as $E_{G/B} = |2\Delta_{so} + E_{qc}|$ in narrow ZXNRs. Here the energy gap

E_{qc} in the subband structure, induced by quantum confinement, is inversely proportional to the ZXNR width.^{19–24}

Low-Voltage topological switching without bulk band gap closing

Similarly to the PT-symmetric case, PT-symmetry breaking via gate electric field also displays interesting features in narrow ZXNRs. As shown in figure 2 (c), (i) the critical gate electric field required for switching between gapless to gapped spin-filtered chiral edge states decreases with decrease in the width, depicted in figure 1 (c), and (ii) the topological switching between gapless and gapped edge state spectrum of narrow ZXNRs is not accompanied by bulk band gap closing and reopening.

First of all, with decreasing ZXNR width, the gate induced anti-crossing points in the edge state spectrum move away from the valleys towards TRIM. Since the momentum space location of anti-crossing points is directly associated with the threshold gate voltage, this voltage decreases as the anti-crossing points move closer to the TRIM. In wide ZXNRs ($N=100$), the spin-filtered Dirac points are gapped out exactly at the valleys K/K' and the SOI induced barrier for critical electric field reads $E_c = 2\Delta_{so}/\alpha_v$. On the other hand, in narrow quantum confined ZXNRs ($N=10,5$), the edge state are gapped out before reaching to the valleys K/K' . As a result, the critical electric field reduces significantly from the SOI driven barrier $E_c < 2\Delta_{so}/\alpha_v$ with decrease in the width. This trend suggests that critical electric field has no lower bound and any nonzero electric field can open an energy gap in the edge state spectrum of ultra-narrow ZXNRs. As discussed later, the decrease in the critical gate electric field is the consequence of non-vanishing overlap integral between spin-filtered edge states associated with momentum lying away from TRIM $k_x = \pi$.

In addition, the evolution of the bulk bands during topological switching from gapless to gapped edge state spectrum looks quite different for wide and narrow ribbons. In wide ZXNRs, during the edge state evolution, the bulk band gap closes at the valleys and the HOMO-LUMO (carrying the same spin as the edge states in particular valleys) of the bulk

band spectrum become valley degenerate with the edge states, and the bulk band gap reopens when $E_c > 2\Delta_{so}/\alpha_v$. It implies that the topological switching via electric field is accompanied by a quantum phase transition between Z_2 -nontrivial and Z_2 -trivial insulating phases where the bulk band gap closes and reopens at the valleys. On the hand, in narrow ZXNRs, transitioning between gapless to gapped edge state spectrum occurs without bulk band gap closing and reopening. The closing and re-opening of bulk band gap is not necessary in narrow ZXNRs, as the 1D system is no longer a 2D topological insulator with a well-defined Z_2 index. Hence no band gap closing and re-opening is needed to switch the topology.

Such finite-size driven topological switching of edge state conductance, without bulk band gap closing and reopening, is an entirely different concept from the previously studied quantum phase transition of the bulk band topology induced by symmetry breaking.³⁶⁻⁴⁰ Since the symmetry class of ZXNRs remains unchanged, irrespective of width, the quantum critical point for transitioning between Z_2 -nontrivial to Z_2 -trivial should remain the same, constrained by the SOI induced barrier. However, apart from SOI terms, quantum confinement induces an extra contribution to the bulk band gap of narrow ZXNRs. Since gate electric field cannot manipulate the band gap due to quantum confinement but the only one induced by SOI, it leads to topological switching of the edge state conductance via spin-filtered chiral modes without bulk band gap closing. The critical electric field reads $E_c^{TS} < E_c^{QPT} = 2\Delta_{so}/\alpha_v$, where the superscript "TS" and "QPT" represent topological switching and quantum phase transition respectively. It shows that the switching without bulk gap closing/reopening is a sheer consequence of the quantum confinement effect on the bulk band spectrum of narrow ZXNRs and can be verified from the calculated band dispersion (2).

Accompanying finite-size effects on the edge state spectrum and quantum confinement effects on the bulk band spectrum, another critical phenomenon occurs, associated with the bulk band spectrum: the Rashba effect. For a specific width of ZXNRs, Rashba SOI further lowers the critical gate electric field via topological quantum field effect on the bulk band

spectrum.¹⁰ For quantum confined spin-orbit coupled ZXNRs, low-energy single-particle electronic dispersion in the vicinity of the Dirac points reads

$$E(k_x) = \pm \sqrt{v_F^2 k_x^2 + v_F^2 k_n^2 + \left| 6\sqrt{3}\lambda_{so} - \alpha_v E_v \left(\frac{1}{2} - \sqrt{\frac{1}{4} + \left(\frac{2\alpha_R}{\alpha_v} \right)^2} \right) \right|^2} \quad (2)$$

where $v_F = \sqrt{3}a_0t/2$ is the Fermi velocity, α_v is the buckling dependent parameter, α_R is a Rashba SOI parameter, and k_n is the quantized transverse momentum along confinement direction. Such finite-size dependent quantization of transverse momentum divides the electronic band dispersion into infinite set of discrete subbands indexed by quantum number $n = 1, 2, 3, \dots$. Specific to our interest in this study, the band dispersion shows that quantum confinement effect induces an additional factor, $v_F^2 k_n^2$, which enhances the bulk band gap. Discretized transverse momentum k_n is related with longitudinal momentum k_x as

$$k_x = \frac{k_n}{\tan(k_n W_z)} \quad (3)$$

Role of intrinsic topology in pristine ZXNRs

The flat bands in the edge state spectrum of pristine ZXNRs are not generated from the intrinsic electronic spectrum of 2D-sheets but are rather indebted to the intrinsic band topology associated with the edge state wave functions. The electronic dispersion of pristine ZXNRs shows that a critical longitudinal momentum $k_x = k_x^c$ divides the momentum space regime for the extended (trivial) and the localized (nontrivial) edge state associated with gapped dispersing and gapless flat bands respectively. Moreover, the nontrivial regime of first Brillouin zone hosting flat bands dwindles with decreases in the width of ZXNRs. That is, with decreasing width of the ZXNR, the location of the critical longitudinal momentum $k_x = k_x^c$ moves towards the TRIM $k_x = \pi$. As a result the critical longitudinal momentum reads $k_x = k_x^c > K$ for narrow ZXNRs, in contrast to $k_x = K$ in wide ZXNRs.

Such finite-size effects on the pristine ZXNRs are intertwined with finite-size effects on

the gate-induced topological switching in spin-orbit coupled ZXNRs. It is interesting to note that the momentum space location of gate-induced anti-crossing points in spin-orbit coupled ZXNRs is exactly same as the critical longitudinal momentum $k_x = k_x^c$ in pristine ZXNRs. At this point the four-fold degenerate energy-zero flat bands in pristine ZXNRs are intrinsically gapped out by finite size effects while the gate-induced two-fold degenerate spin-filtered Dirac points in spin-orbit coupled ZXNRs are gapped out by the dominating gate electric field. It implies that the reduction of critical gate electric field in the spin-orbit coupled ZXNRs is intrinsically associated with the finite-size effects on the nontrivial character of pristine ZXNRs rather than mere manipulation of intrinsic SOI. More specifically, the impact of intrinsic band topology of pristine ZXNRs on the electronic properties of spin-orbit coupled ZXNRs can be summarized as follows: in the nontrivial regime, while the critical momentum space location k_x^c depends on the width of ZXNR, the strength of critical gate electric field E_c depends upon both the strength of SOI and the width of ZXNRs. This effect is further demonstrated by studying the real space wave functions for edge states, as shown below, that the reduction in the critical gate electric field is associated with gate-induced longitudinal momentum-dependence of inter-edge coupling in the vicinity of k_x^c .

Width/Momentum dependence of edge states

In order to understand how the longitudinal momentum-dependence of inter-edge coupling guarantees the protection of conducting edge states and assists electric field driven topological switching, we investigate the real-space wave functions for the edge states near the Fermi energy of a spin-orbit coupled ZXNR terminated at A and B sublattice sites respectively. As shown in figure 2, the spin-filtered chiral edge states are characterized by a range of longitudinal momentum $k_x \in (2\pi/3a_0, 4\pi/3a_0)$, defining a nontrivial regime of first Brillouin zone. In the vicinity of valleys $k_x \approx 2\pi/3a_0$ and $k_x \approx 4\pi/3a_0$, as depicted in figure 3(a-c), the real-space squared wave function decay exponentially along the confined direction

and have finite overlapping. With decrease in width, though the amplitude near the edges increases, overlapping between edge states at the two sides of ZXNRs also increases. As one moves away from valleys towards TRIM $k_x = \pi$, due to large probability distribution near the edges, amplitude of squared wave functions increases while the decay length decreases. For example, as shown in figure 3(d-f), nearly orthogonal squared wave functions indicate that the penetration depth of exponentially decaying edge states becomes much smaller than those around valleys K/K' . Associated with longitudinal momentum around the TRIM $k_x = \pi$, as shown in figure 3(g-i), spin-filtered chiral edge states distributed near the edges appear to be completely orthogonal and hence the inter-edge overlap integral remain zero even for ultra narrow ZXNRs.

Accuracy of numerical tight binding results, describing the longitudinal momentum dependence of edge states in quantum confined ZXNRs, can be probed by obtaining the explicit expressions of the wave functions for the spin-filtered chiral edge states via analytically solving tight binding model.⁴¹ Based on the nature of wave functions, edge state spectrum in ZXNRs can be divided into three regimes of momentum space: (i) In region I, in the vicinity of TRIM $k_x \approx \pi$ where edge spectrum forms four-fold degenerate Dirac point in the absence of gate electric field, the wave functions are damped oscillatory. (ii) In region II, $k_x \in [2\pi/3a_0, \pi) \cup (\pi, 4\pi/3a_0]$ lying between the Dirac points, the wave functions at the edges decay exponentially along the confined direction. (iii) In region III, away from Dirac point $2\pi/3a_0 > k_x > 4\pi/3a_0$, the wave functions are oscillatory in nature and represent the localized 1D edge states due to admixing with bulk subbands. It implies that the spin-filtered chiral edge states are formed by a combination of wave functions in the region I and II and the nature of these wave functions changes from exponentially decaying to damped oscillatory as k_x moves from region II to region I. Analytical tight binding results in region I and II are shown in the insets of figure 3.

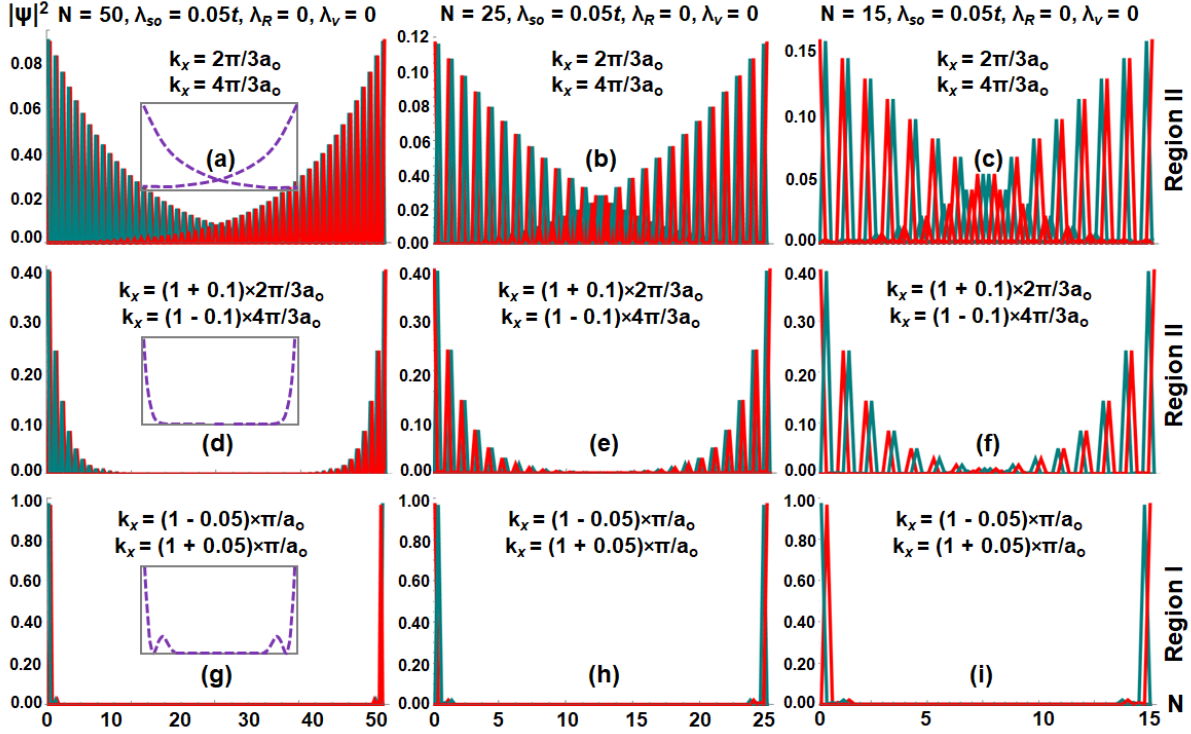


Figure 3: **Longitudinal momentum and width dependence of real-space squared wave functions for the spin-filtered chiral edge states.** Real-space squared wave function for the spin-filtered chiral edge states near the Fermi energy of a ZXNRs with longitudinal momentum lying at Dirac/valley points $k_x = 2\pi/3a_0$ (a-c), away from Dirac points in the nontrivial regime (d-f), and in the vicinity of TRIM $k_x \approx \pi/a_0$ (g-i). The insets, dashed curves which are consistent with analytical tight binding model calculations, show that edge states are damped oscillatory in region I (g-i) while the edge states decay exponentially for momentum away from TRIM, in region II (a-f). For a fixed N , decay length of edge state decreases as k_x moves from valleys towards the TRIM (from top to bottom). While there is no inter-edge overlapping in region I, finite inter-edge overlapping in region II increases with decrease in width (a-c). Here SOI parameters are taken as $\lambda_{so}/t = 0.05$ and $\lambda_R = 0$ in the absence of gate potential $\lambda_v = 0$. The horizontal axis is the confinement direction, along y -axis of the zigzag 2D-Xenes nanoribbon here.

This analysis leads to three important outcomes: (i) classification of edge states longitudinal momentum k_x shows that the edge states in ZXNRs are similar to those in a conventional quantum Hall strip where translational symmetry is preserved along the strip. The spin-filtered chiral edge states along the two sides of ZXNRs are associated with different k_x and do not hybridize with each other even when there is a finite overlap along the confined direction in region II.^{42,43} On the other hand, in region I where the energy

and momentum of edge states around the crossing point $k_x = \pi$ is nearly equal and they can possibly couple to open an energy gap, their wave functions do not overlap in a finite space. It implies that, in the absence of gate electric field, spin-filtered chiral edge states do not hybridize/couple even in ultra narrow ZXNRs. (ii) Resemblance of damped oscillatory behavior around $k_x = \pi$ to the one in spin-orbit coupled armchair 2D-Xenes nanoribbons (AXNR)⁴⁴ suggests that the dynamical evolution of edge states remain independent of particular edge termination in region I. On the other hand, the exponentially decaying wave functions in region II are directly associated with the particular edge termination on A and B sublattice sites and hence can be tuned via gate induced staggered sublattice potentials. (iii) In region II, increase in overlap between inter-edge states with decreases in width indicates the enhancement of gate-induced inter-edge coupling in narrow ZXNRs. That is, with decrease in width, gate-induced anti-crossing points move away from valleys and hence the threshold voltages decreases.

Width/Momentum dependence of gate-induced inter-edge coupling

To further investigate the dependence of gate electric field effect on the longitudinal momentum k_x , we study the gate electric field modulation of edge states wave functions associated with various longitudinal momentum. As shown in figure 4 (g-i), our numerical calculations show that the damped oscillatory edge states in region I remains insensitive to the gate electric field, i.e., penetration depth remains same and both the spin up and down edge states remain damped oscillatory and traversing along the edges even for very large gate electric field. On the other hand, as shown in figure 4 (a-f), exponentially decaying edge states in region II are highly sensitive to the gate electric field effects. First of all, In the vicinity of momentum $k_x \approx 5\pi/6a_0$ as shown in figure 4 (d-f), gate electric field hybridizes spin-down edge states while amplitude of spin-up edge states decreases with increasing electric field but

they remain uncoupled. It implies that, spin up edge states remain exponentially decaying and traversing while spin down edge states become sinusoidal and gapped in this regime of longitudinal momentum, consistent with tight binding electronic dispersion. As one moves towards the valley $k_x \approx 2\pi/3a_0$ as shown in figure 4(a-c), it can be clearly seen that gate electric field induces coupling between overlapping exponentially decaying wave functions in both spin up and down sectors and localizes them. The period of these exponentially turned sinusoidal wave functions decreases with increase in gate voltage. Similar gate controlled edge state dynamics appears on the other valley, $k_x \approx 4\pi/3a_0$, but the spin character is interchanged due to electric field induced spin-valley locking.

Based on the edge state dynamics, we came to a following conclusion: In the absence of gate electric field, non-vanishing overlap between edge states in region II do not hybridize/couple to open energy gap as they lie at different longitudinal momenta. However, mainly due to spin-valley locking, gate electric field splits four-fold degenerate Dirac point in region I and moves the spin-polarized two-fold Dirac points towards region II. The finite inter-edge overlapping in region II allows gate electric field to induce coupling between spin-filtered inter-edge states. Within the accuracy of electronic dispersion and edge state wave functions found via numerical tight binding approximations, since the inter-edge overlapping increases with decrease in width as shown in figure 3 (a-f), gate electric field utilizes such enhancement of penetration depth and hence the inter-edge overlapping in the region II to lower the critical gate electric field required for topological switching between gapless to gapped edge states.

These numerical tight binding calculations are consistent with analytical results: while the dynamical evolution of edge states remain independent of particular edge termination in region I, exponentially decaying wave functions in region II are directly associated with the particular edge termination on A and B sublattice sites and hence their penetration depth can be tuned via gate induced staggered sublattice potentials. The consistency of both numerical and analytical tight binding results indicates that the finite-size effect assistance in

the topological switching is the artefact of this gate-induced momentum-dependent coupling between wave functions along the edges.

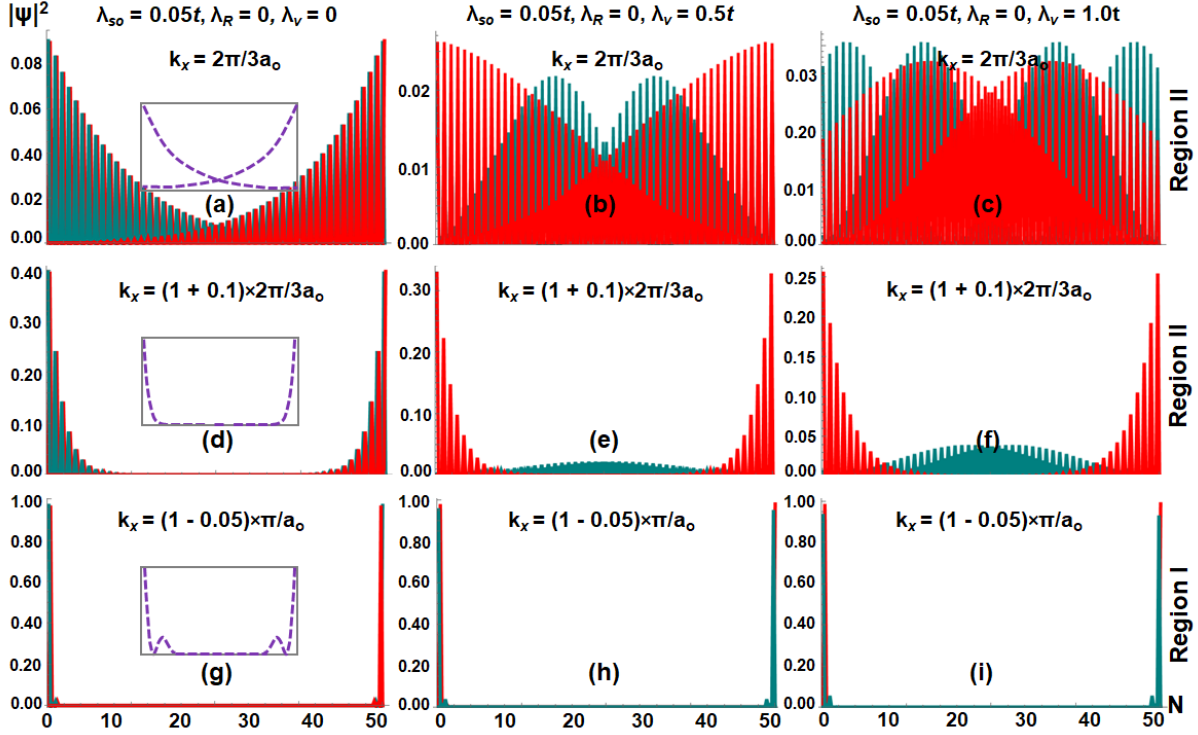


Figure 4: **Longitudinal momentum and width dependence of gate-induced inter-edge coupling.** For a fixed width $N=50$, effect of gate electric field on real-space squared wave function for the spin-filtered chiral edge states associated with longitudinal momentum k_x lying in region II (a-f) and region I, in the vicinity of TRIM $k_x \approx \pi/a_0$ (g-i). In the vicinity of Dirac/valley point $k_x = 2\pi/3a_0$ (a-c), critical gate electric field localizes both the spin-down and spin-up sectors by turning exponentially decaying edge states into sinusoidal form. Such gate-induced enhancement in the penetration depth of chiral edge states and the gate-induced inter-edge coupling leads to an energy gap in the edge state spectrum when gate electric field exceeds critical limit. As one moves away from Dirac point, $k_x \approx 5\pi/6a_0$ (d-f), similar evolution occurs in spin-down sector but the spin-up sector remains always exponentially decaying and traversing. In region I (g-i), in the vicinity of TRIM $k_x = \pi/a_0$, penetration depth of edge states remains insensitive to gate electric field effect and both the spin up and the spin down chiral edge states remains traversing along the edges even for quite large gate electric field. Here SOI parameters are taken as $\lambda_{so}/t = 0.05$ and $\lambda_R = 0$. The horizontal axis is the confinement direction, along y-axis of the nanoribbon here.

Effect of electron-electron Coulomb interactions

Furthermore, though the electron-electron Coulomb interactions become inevitable in quantum confined ZXNRs, spin-filtered chiral edge conducting channels may remain gapless even when both intra- and inter-edge Coulomb interactions are present. For example, contrary to pristine ZXNRs where Coulomb interactions leads to energy gap by lifting the four-fold degeneracy of energy-zero flat bands in the edge state spectrum,^{45–47} it has been explicitly shown that QSH phase in spin-orbit coupled ZXNRs remain stabilized against intra-edge Coulomb interactions.⁴⁸ Moreover, the mass term produced by backward scattering, which may be originated from the mixing of right and left moving chiral modes carrying same spin polarization and located at opposite edges of finite-size ZXNRs, can be suppressed in the large SOI limit and hence the spin-filtered chiral edge states may also remain protected against unscreened inter-edge Coulomb interactions.⁴¹ It can be justified by a simple argument based on the interplay between strength of intrinsic SOI and the screening length of Coulomb interactions: since the decay length of spin-filtered chiral edge states in ZXNRs is inversely proportional to the intrinsic SOI, the overlaps between oppositely moving spin-filtered chiral modes are suppressed with increasing SOI. It shows that, in the large SOI limit, even ultra-narrow ZXNRs can be described by tight binding model where both intra- and inter-edge Coulomb interactions are effectively absent. Thus, even in the presence of Coulomb interactions, large SOI limit renders gapless spin-filtered chiral edge states since the reduced inter-edge overlap diminishes the backward scattering terms.

Based on the similar argument, our findings provide another ground: In the QSH phase, spin-filtered chiral states associated with longitudinal momentum $k_x = \pi$ in region I remain protected against backward scattering due to vanishing inter-edge overlap. On the other hand, in the presence of gate electric field, unscreened inter-edge Coulomb interactions may also assist the topological switching by inducing energy gap due to finite inter-edge coupling between edge states associated with longitudinal momentum k_x lying in region II of Brillouin zone, similar to finite-size effect. In passing, unlike finite-size effect which is characterised

by critical longitudinal momentum k_x^c and remains same in both pristine and spin-orbit coupled ZXNRs, effect of Coulomb interactions in pristine ZXNRs is completely different from spin-orbit coupled ZXNRs.

Low-voltage topological quantum devices

Analogy between rich momentum-dependent behaviour of edge states and the gate-controlled inter-edge coupling in the spin-orbit coupled ZXNRs leads to following two phenomena which are critical for topological quantum devices: (i) In the absence of gate electric field and hence Rashba SOI, spin-filtered chiral edge edge states with four-fold degenerate Dirac point at TRIM $k_x = \pi$ remain gapless even for ultra-narrow ZXNRs. Vanishing inter-edge coupling across the crossing point guarantees that the spin-filtered chiral edge states (enabling dissipationless and quantized conductance) remain topologically protected against backscattering and hence the deviation from conductance quantization - a figure of merit in QSH materials. (ii) Since the gate electric field splits four-fold Dirac point at TRIM and moves spin-filtered two-fold Dirac points towards valleys, gate-induced coupling due to finite overlap between spin-filtered inter-edge states across anti-crossing points assist in opening energy gap in the spin-filtered chiral edge states and lowers the critical gate electric field. This artefact of finite-size effect, dwindled nontrivial regime of Brillouin zone without affecting bulk band topology and reduced critical gate electric field without affecting the quantized edge state conductance in QSH phase, provide ideal platform for devising energy-efficient low-voltage topological quantum devices.

Optimization of topological switching via finite-size effects is a purely quantum mechanical phenomenon associated with QSH materials with honeycomb lattice structures and has no counterpart in conventional semiconducting technologies. In conventional switching devices utilizing Z_2 -trivial semiconductors, finite size effects enhance both the band gap and hence the threshold gate voltage. In other words, threshold gate voltage enhances with

decrease in width of Z_2 -trivial channel, known as narrow-width effect. As a result, only possible strategies to lower the threshold gate voltage resort to the configuration of wide channel and narrow gap conventional semiconductors. However, by configuring Z_2 -nontrivial QSH materials, we show that the threshold gate voltage reduces with decrease in channel width even though the topological bulk band gap increases due to quantum confinement effect. Such completely contrasting role of finite-size effects in topological quantum materials is indebted to the gate electric field driven topological switching which is a fundamentally different mechanism of operation compared to a traditional carrier inversion in conventional semiconducting switching devices. In summary, our work overturns conventional wisdom of utilizing wide channel and narrow gap semiconductors for reducing threshold gate voltage in standard field effect transistor analysis, demonstrating that it can be resorted to finite-size effect assisted topological switching with large band gap in quantum confined narrow ribbons of QSH materials.

Conclusion

It is demonstrated that, in a finite-size geometry, ZXNRs display unique physical characteristics associated with intrinsic band topology and the finite-size effects such as longitudinal momentum dependent inter-edge overlapping between spin-filtered chiral edge states and the quantum confinement effect on the bulk band spectrum. While the damped oscillatory modes around the edge state crossing momenta remain completely orthogonal and guarantee protected spin-filtered chiral edge states even in the ultra-narrow ribbons, enhanced gate-induced inter-edge coupling between exponentially decaying edge states around the anti-crossing points reduces gate electric field required for topological switching between gapless to gapped edge states. In addition, quantum confinement effect enhances the SOI induced band gap in the nontrivial phase and leads to topological switching without bulk band gap closing. Furthermore, similar to wide ZXNRs, Rashba effect enhances the band gap in the

trivial phase. Hence, a large nontrivial bulk band gap by quantum confinement effect to decouple the conducting edge states from bulk subbands and a large trivial band gap by Rashba effect to overcome thermal excitation makes quantum confined narrow ZXNRs ideal for engineering energy-efficient low-voltage topological quantum devices.

In passing, it is noted and will be presented in a separate study, longitudinal momentum and width dependence of gate-induced inter-edge coupling can also be employed to tune the exchange interaction in 2D magnetic topological insulators.^{49–57} For example, critical regime in an antiferromagnetic topological insulators can be optimized to design a topological spin transistor via gate induced topological switching of edge state spin transport. Furthermore, this study may also help in optimizing the topological protection of Majorana bound states localized along the edges of topological superconductors with finite-size geometry.^{58–60}

Acknowledgements

This research is supported by the Australian Research Council (ARC) Centre of Excellence in Future Low-Energy Electronics Technologies (FLEET Project No. CE170100039), Australian Research Council (ARC) Professional Future Fellowship (FT130100778), and funded by the Australian Government.

References

- (1) Seidel, J. Nanoelectronics based on topological structures. *Nature Materials* **2019**, *18*, 188–190.
- (2) Ezawa, M. Quantized conductance and field-effect topological quantum transistor in silicene nanoribbons. *Applied Physics Letters* **2013**, *102*, 172103.
- (3) Liu, J.; Hsieh, T. H.; Wei, P.; Duan, W.; Moodera, J.; Fu, L. Spin-filtered edge states

- with an electrically tunable gap in a two-dimensional topological crystalline insulator. *Nature Materials* **2014**, *13*, 178–183.
- (4) Liu, Q.; Zhang, X.; Abdalla, L. B.; Fazio, A.; Zunger, A. Switching a Normal Insulator into a Topological Insulator via Electric Field with Application to Phosphorene. *Nano Letters* **2015**, *15*, 1222–1228, PMID: 25607525.
- (5) Pan, H.; Wu, M.; Liu, Y.; Yang, S. A. Electric control of topological phase transitions in Dirac semimetal thin films. *Scientific Reports* **2015**, *5*, 14639.
- (6) Qian, X.; Liu, J.; Fu, L.; Li, J. Quantum spin Hall effect in two-dimensional transition metal dichalcogenides. *Science* **2014**, *346*, 1344–1347.
- (7) Zhang, Z.; Feng, X.; Wang, J.; Lian, B.; Zhang, J.; Chang, C.; Guo, M.; Ou, Y.; Feng, Y.; Zhang, S.-C.; He, K.; Ma, X.; Xue, Q.-K.; Wang, Y. Magnetic quantum phase transition in Cr-doped $Bi_2(Se_xTe_{1-x})_3$ driven by the Stark effect. *Nature Nanotechnology* **2017**, *10*, 953–957.
- (8) Molle, A.; Goldberger, J.; Houssa, M.; Xu, Y.; Zhang, S.-C.; Akinwande, D. Buckled two-dimensional Xene sheets. *Nature Materials* **2017**, *16*, 163–169.
- (9) Collins, J. L.; Tadich, A.; Wu, W.; Gomes, L. C.; Rodrigues, J. N. B.; Liu, C.; Hellerstedt, J.; Ryu, H.; Tang, S.; Mo, S.-K.; Adam, S.; Yang, S. A.; Fuhrer, M. S.; Edmonds, M. T. Electric-field-tuned topological phase transition in ultrathin Na_3Bi . *Nature* **2018**, *564*, 390–394.
- (10) Nadeem, M.; Di Bernardo, I.; Wang, X.; Fuhrer, M. S.; Culcer, D. Overcoming Boltzmann’s Tyranny in a Transistor via the Topological Quantum Field Effect. *Nano Letters* **2021**, *21*, 3155–3161, PMID: 33780625.
- (11) Xu, Y.; Chen, Y.-R.; Wang, J.; Liu, J.-F.; Ma, Z. Quantized Field-Effect Tunneling between Topological Edge or Interface States. *Phys. Rev. Lett.* **2019**, *123*, 206801.

- (12) Bernevig, B. A.; Hughes, T. L.; Zhang, S.-C. Quantum Spin Hall Effect and Topological Phase Transition in HgTe Quantum Wells. *Science* **2006**, *314*, 1757–1761.
- (13) König, M.; Buhmann, H.; W. Molenkamp, L.; Hughes, T.; Liu, C.-X.; Qi, X.-L.; Zhang, S.-C. The Quantum Spin Hall Effect: Theory and Experiment. *Journal of the Physical Society of Japan* **2008**, *77*, 031007.
- (14) Shan, W.-Y.; Lu, H.-Z.; Shen, S.-Q. Effective continuous model for surface states and thin films of three-dimensional topological insulators. *New Journal of Physics* **2010**, *12*, 043048.
- (15) Liu, C.-X.; Zhang, H.; Yan, B.; Qi, X.-L.; Frauenheim, T.; Dai, X.; Fang, Z.; Zhang, S.-C. Oscillatory crossover from two-dimensional to three-dimensional topological insulators. *Phys. Rev. B* **2010**, *81*, 041307.
- (16) Lu, H.-Z.; Shan, W.-Y.; Yao, W.; Niu, Q.; Shen, S.-Q. Massive Dirac fermions and spin physics in an ultrathin film of topological insulator. *Phys. Rev. B* **2010**, *81*, 115407.
- (17) Zhou, B.; Lu, H.-Z.; Chu, R.-L.; Shen, S.-Q.; Niu, Q. Finite Size Effects on Helical Edge States in a Quantum Spin-Hall System. *Phys. Rev. Lett.* **2008**, *101*, 246807.
- (18) Das, B.; Sen, D.; Mahapatra, S. Tuneable quantum spin Hall states in confined 1T' transition metal dichalcogenides. *Scientific Reports* **2020**, *10*, 6670.
- (19) Ezawa, M. Peculiar width dependence of the electronic properties of carbon nanoribbons. *Phys. Rev. B* **2006**, *73*, 045432.
- (20) Han, M. Y.; Özyilmaz, B.; Zhang, Y.; Kim, P. Energy Band-Gap Engineering of Graphene Nanoribbons. *Phys. Rev. Lett.* **2007**, *98*, 206805.
- (21) Son, Y.-W.; Cohen, M. L.; Louie, S. G. Energy Gaps in Graphene Nanoribbons. *Phys. Rev. Lett.* **2006**, *97*, 216803.

- (22) Brey, L.; Fertig, H. A. Electronic states of graphene nanoribbons studied with the Dirac equation. *Phys. Rev. B* **2006**, *73*, 235411.
- (23) Ezawa, M.; Nagaosa, N. Interference of topologically protected edge states in silicene nanoribbons. *Phys. Rev. B* **2013**, *88*, 121401.
- (24) Cano-Cortés, L.; Ortix, C.; van den Brink, J. Fundamental Differences between Quantum Spin Hall Edge States at Zigzag and Armchair Terminations of Honeycomb and Ruby Nets. *Phys. Rev. Lett.* **2013**, *111*, 146801.
- (25) Kane, C. L.; Mele, E. J. Z_2 Topological Order and the Quantum Spin Hall Effect. *Phys. Rev. Lett.* **2005**, *95*, 146802.
- (26) Kane, C. L.; Mele, E. J. Quantum Spin Hall Effect in Graphene. *Phys. Rev. Lett.* **2005**, *95*, 226801.
- (27) Min, H.; Hill, J. E.; Sinitsyn, N. A.; Sahu, B. R.; Kleinman, L.; MacDonald, A. H. Intrinsic and Rashba spin-orbit interactions in graphene sheets. *Phys. Rev. B* **2006**, *74*, 165310.
- (28) Liu, C.-C.; Feng, W.; Yao, Y. Quantum Spin Hall Effect in Silicene and Two-Dimensional Germanium. *Phys. Rev. Lett.* **2011**, *107*, 076802.
- (29) Liu, C.-C.; Jiang, H.; Yao, Y. Low-energy effective Hamiltonian involving spin-orbit coupling in silicene and two-dimensional germanium and tin. *Phys. Rev. B* **2011**, *84*, 195430.
- (30) Xu, Y.; Yan, B.; Zhang, H.-J.; Wang, J.; Xu, G.; Tang, P.; Duan, W.; Zhang, S.-C. Large-Gap Quantum Spin Hall Insulators in Tin Films. *Phys. Rev. Lett.* **2013**, *111*, 136804.
- (31) Hsu, C.-H.; Huang, Z.-Q.; Chuang, F.-C.; Kuo, C.-C.; Liu, Y.-T.; Lin, H.; Bansil, A.

- The nontrivial electronic structure of Bi/Sb honeycombs on SiC(0001). *New Journal of Physics* **2015**, *17*, 025005.
- (32) Reis, F.; Li, G.; Dudy, L.; Bauernfeind, M.; Glass, S.; Hanke, W.; Thomale, R.; Schäfer, J.; Claessen, R. Bismuthene on a SiC substrate: A candidate for a high-temperature quantum spin Hall material. *Science* **2017**, *357*, 287–290.
- (33) Li, G.; Hanke, W.; Hankiewicz, E. M.; Reis, F.; Schäfer, J.; Claessen, R.; Wu, C.; Thomale, R. Theoretical paradigm for the quantum spin Hall effect at high temperatures. *Phys. Rev. B* **2018**, *98*, 165146.
- (34) Salahuddin, S.; Datta, S. Use of Negative Capacitance to Provide Voltage Amplification for Low Power Nanoscale Devices. *Nano Letters* **2008**, *8*, 405–410, PMID: 18052402.
- (35) Rashba, E. I. Graphene with structure-induced spin-orbit coupling: Spin-polarized states, spin zero modes, and quantum Hall effect. *Phys. Rev. B* **2009**, *79*, 161409.
- (36) Ezawa, M.; Tanaka, Y.; Nagaosa, N. Topological Phase Transition without Gap Closing. *Scientific Reports* **2013**, *3*, 2790.
- (37) Yang, Y.; Li, H.; Sheng, L.; Shen, R.; Sheng, D. N.; Xing, D. Y. Topological phase transitions with and without energy gap closing. *New Journal of Physics* **2013**, *15*, 083042.
- (38) Rachel, S. Quantum phase transitions of topological insulators without gap closing. *Journal of Physics: Condensed Matter* **2016**, *28*, 405502.
- (39) Matsumoto, N.; Kawabata, K.; Ashida, Y.; Furukawa, S.; Ueda, M. Continuous Phase Transition without Gap Closing in Non-Hermitian Quantum Many-Body Systems. *Phys. Rev. Lett.* **2020**, *125*, 260601.
- (40) Schindler, F. Dirac equation perspective on higher-order topological insulators. *Journal of Applied Physics* **2020**, *128*, 221102.

- (41) Zarea, M.; Büsser, C.; Sandler, N. Unscreened Coulomb Interactions and the Quantum Spin Hall Phase in Neutral Zigzag Graphene Ribbons. *Phys. Rev. Lett.* **2008**, *101*, 196804.
- (42) Halperin, B. I. Quantized Hall conductance, current-carrying edge states, and the existence of extended states in a two-dimensional disordered potential. *Phys. Rev. B* **1982**, *25*, 2185–2190.
- (43) MacDonald, A. H.; Středa, P. Quantized Hall effect and edge currents. *Phys. Rev. B* **1984**, *29*, 1616–1619.
- (44) Zarea, M.; Sandler, N. Electron-Electron and Spin-Orbit Interactions in Armchair Graphene Ribbons. *Phys. Rev. Lett.* **2007**, *99*, 256804.
- (45) Hikihara, T.; Hu, X.; Lin, H.-H.; Mou, C.-Y. Ground-state properties of nanographite systems with zigzag edges. *Phys. Rev. B* **2003**, *68*, 035432.
- (46) Son, Y.-W.; Cohen, M. L.; Louie, S. G. Energy Gaps in Graphene Nanoribbons. *Phys. Rev. Lett.* **2006**, *97*, 216803.
- (47) Yang, L.; Park, C.-H.; Son, Y.-W.; Cohen, M. L.; Louie, S. G. Quasiparticle Energies and Band Gaps in Graphene Nanoribbons. *Phys. Rev. Lett.* **2007**, *99*, 186801.
- (48) Xu, C.; Moore, J. E. Stability of the quantum spin Hall effect: Effects of interactions, disorder, and Z_2 topology. *Phys. Rev. B* **2006**, *73*, 045322.
- (49) Ezawa, M. Spin valleytronics in silicene: Quantum spin Hall–quantum anomalous Hall insulators and single-valley semimetals. *Phys. Rev. B* **2013**, *87*, 155415.
- (50) Ezawa, M. Topological Kirchhoff law and bulk-edge correspondence for valley Chern and spin-valley Chern numbers. *Phys. Rev. B* **2013**, *88*, 161406.
- (51) Ezawa, M. Monolayer Topological Insulators: Silicene, Germanene, and Stanene. *Journal of the Physical Society of Japan* **2015**, *84*, 121003.

- (52) Högl, P.; Frank, T.; Zollner, K.; Kochan, D.; Gmitra, M.; Fabian, J. Quantum Anomalous Hall Effects in Graphene from Proximity-Induced Uniform and Staggered Spin-Orbit and Exchange Coupling. *Phys. Rev. Lett.* **2020**, *124*, 136403.
- (53) Li, X.; Cao, T.; Niu, Q.; Shi, J.; Feng, J. Coupling the valley degree of freedom to antiferromagnetic order. *Proceedings of the National Academy of Sciences* **2013**, *110*, 3738–3742.
- (54) Liang, Q.-F.; Wu, L.-H.; Hu, X. Electrically tunable topological state in [111] perovskite materials with an antiferromagnetic exchange field. *New Journal of Physics* **2013**, *15*, 063031.
- (55) Zhou, T.; Cheng, S.; Jiang, H.; Yang, Z.; Zutic, I. Quantum Spin-Valley Hall Kink States: From Concept to Realization. *arXiv:2102.05806* **2021**,
- (56) Shabbir, B.; Nadeem, M.; Dai, Z.; Fuhrer, M. S.; Xue, Q.-K.; Wang, X.; Bao, Q. Long range intrinsic ferromagnetism in two dimensional materials and dissipationless future technologies. *Applied Physics Reviews* **2018**, *5*, 041105.
- (57) Nadeem, M.; Hamilton, A. R.; Fuhrer, M. S.; Wang, X. Quantum Anomalous Hall Effect in Magnetic Doped Topological Insulators and Ferromagnetic Spin-Gapless Semiconductors—A Perspective Review. *Small* **2020**, *16*, 1904322.
- (58) San-Jose, P.; Lado, J. L.; Aguado, R.; Guinea, F.; Fernández-Rossier, J. Majorana Zero Modes in Graphene. *Phys. Rev. X* **2015**, *5*, 041042.
- (59) Ezawa, M. Antiferromagnetic Topological Superconductor and Electrically Controllable Majorana Fermions. *Phys. Rev. Lett.* **2015**, *114*, 056403.
- (60) Potter, A. C.; Lee, P. A. Multichannel Generalization of Kitaev’s Majorana End States and a Practical Route to Realize Them in Thin Films. *Phys. Rev. Lett.* **2010**, *105*, 227003.